Applied Binary Star Research

Binary star observations with interferometers serve a number of interests, and present a number of challenges; amongst them are:

- **Imaging**. Binaries have the most simple non-trivial stellar structure; imaging speeds up modeling process; challenges include bandwidth synthesis and orbital motion.
- **Fundamental stellar parameters**. Binaries allow the determination of masses, luminosities, and radii of the constituent component stars; a challenge is to achieve the required accuracies.
- **Orbital parameters**. Interests include their distributions, and extremes.
- **Binary star frequency and formation**. Multiple-star formation is an important theoretical challenge as only a minority of the stars in the universe are single.

Further reading (unless noted in text):

- **Hipparcos observations of binaries**
  - Martin, C., et al. 1997, A&AS, 122, 571
  - Martin, C., & Mignard, F. 1998, A&A, 330, 585
  - Martin, C., et al. 1998, A&AS, 133, 149
  - Söderhjelm, S. 1999, A&A, 341, 121
- **Speckle**
  - CHARA, McAlister, Hartkopf, Mason, et al.
    "Binary star orbits from speckle interferometry. I – XII."
  - USNO, Worley, Douglass, Mason, Hartkopf, et al.
  - Torres, G., et al. 1997, ApJ, 474, 256
  - Scarfe, C., et al. 1994, AJ, 107, 1529
  - McAlister, H. A. 1996, *Sky and Telescope*, 92, 5/28
- **Conference proceedings**
  - IAU Symposium 200, "The Formation of Binary Stars", to be published by ASP Conference Series.
  - IAU Colloquium 135, "Complementary Approaches to Double and Multiple Star Research", ed. by H.A. McAlister and W.I. Hartkopf, ASP Conference Series Vol 32
  - NATO ASI Series C, Vol 477, "Evolutionary Processes in Binary Stars", ed. by R.A.M.J. Wijers, M.B. Davies, and C.A. Tout, Kluwer: Dordrecht
  - IAU Symposium 189, "Fundamental Stellar Properties: The Interaction between Observation and Theory", ed. by T.R. Bedding A.J. Booth, and J. Davis, Kluwer: Dordrecht

Stellar model and evolution

Johannes Andersen (2000, in "Unsolved problems in stellar evolution", CUP):

> It is elementary textbook material that direct empirical mass determinations are only possible for stars in binary systems (and for the Sun). What is not elementary is how to determine individual masses and radii for stars in binary systems such that these data may help address some of the current unsolved problems in stellar evolution.

Fundamental stellar parameters, i.e. the parameters which uniquely specify an evolutionary model:

- **Mass**
- **Chemical composition**
- **Angular momentum**

Other fundamental properties, observable and predicted by evolutionary models:

- Luminosity
- Effective temperature
- Radius
- Surface gravity

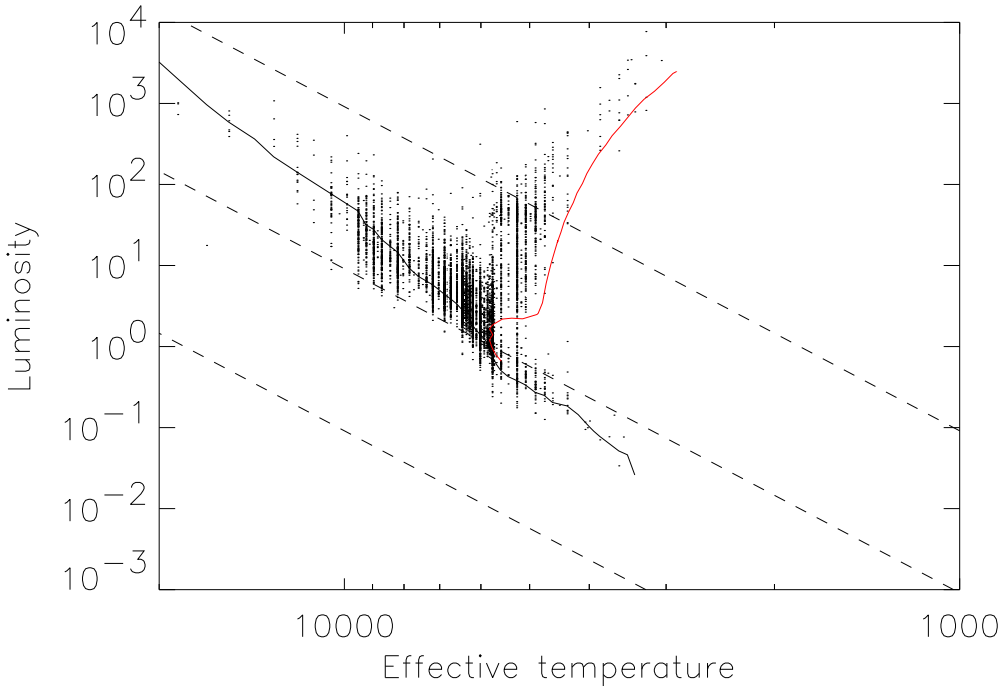

Theoretical Hertzsprung-Russell diagram. Solid line is Zero-age-mainsequence (ZAMS). Dashed lines are blackbody stars of constant radius, the middle line corresponding to the solar radius. The red line is an example for an evolutionary track of a star of one solar mass.

Inventory of masses and luminosities – Optical Interferometry of SB2's (Mark III, NPOI, PTI)

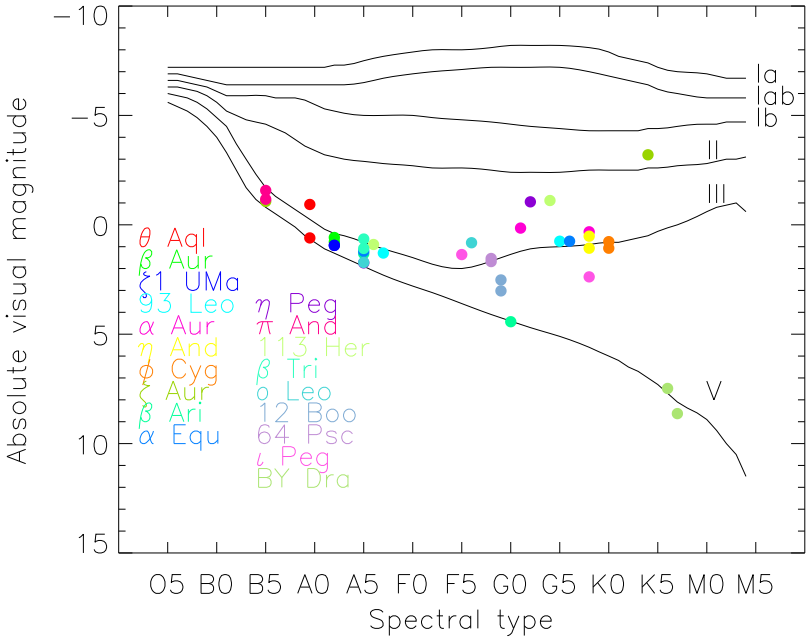

Selected references for high precision masses (% mass/ % luminosity σ):

Armstrong J.T., et al. 1992, AJ, 104, 2217 (ϕ Cygni, 3.3%/12%)
Hummel, C. A., et al. 1995, AJ, 110, 376 (β Aur, 1.2%/7%)
Hummel, C. A., et al. 1998, AJ 116, 2536 (ζ 1 UMa, 2.8%/6.3%)
Hummel, C. A., et al. 1994, AJ, 107, 1859 (α Aur, 1.6–2.2%/1.5–3.3%)
Boden, A. F., et al. 1999, ApJ, 515, 356 (ι Peg, 1.1%/2.5%)
Boden, A. F., et al. 1999, ApJ, 527, 360 (64 Psc, 1.6%/9%)
Boden, A. F., et al. 2000, ApJ, 536, 880 (12 Boo, 1.5%/7%)

Comparison of Hipparcos parallaxes with orbital parallaxes [mas]

Star	HIC	M3/PTI/NPOI	±	Hipparcos	±
θ Aql	99473	13	1	11.4	0.9
β Aur	28360	40	1	39.7	0.8
93 Leo	57565	13.8	0.5	14.4	0.9
η And	4463	13.1	0.3	13.4	0.7
β Ari	8903	53	2	54.7	0.8
β Per	14576	35.4	1.1	35.1	0.9
α Equ	104987	18.1	0.8	17.5	0.9
ζ Aur	23453	3.8	0.1	4.1	0.8
ϕ Cyg	96683	12.4	0.3	13.0	0.6
θ^2 Tau	20894	21.2	0.8	21.9	0.8
α Aur	24608	75.1	0.5	77.3	0.9
Mizar A	65378	39.4	0.3	41.7	0.6
64 Psc	3810	43.3	0.5	41.8	0.8
ι Peg	109176	86.9	1.0	85.1	0.7
12 Boo	69226	27.1	0.4	27.3	0.8
o Leo	47508	24.2	0.1	24.1	1.0

Inventory of precise masses and luminosities – EB

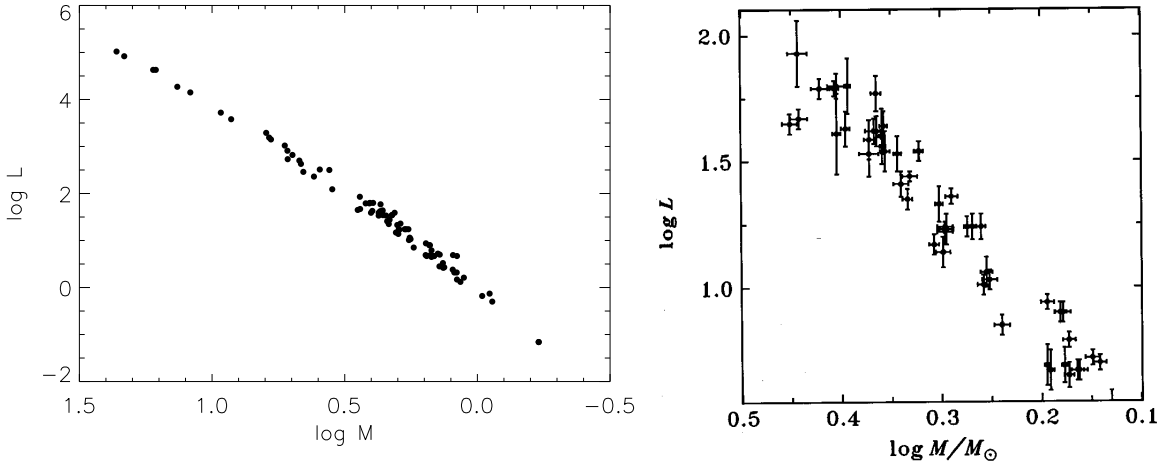

The mass-luminosity relationship after Andersen, 1991, based on observations of eclipsing binaries. On the right is a zoom-in on a section of the diagram, showing that the scatter considerably exceeds the observational errors.

Typical properties of a well studied binary system (after Andersen 1995, IAU 166)

- Mass: 1%
- Radius: 1%
- Luminosity: 10%
- Distance: 3%

Selected references

- Andersen, J. 1991, *Astron. Astrophys. Rev.*, 3, 91
  "Absolute dimensions of eclipsing binaries. I — XXIII."
  A collaboration with Nordström, Clausen, Torres, Stefanik, Latham et al.
- Andersen, J., et al. 1989, A&A, 211, 346
- Casey, W., et al. 1998, AJ, 115, 1617
- Torres, G., et al. 2000, AJ, 119, 1942

$K_{1,2}$, a'': o **Leonis**

"Classical" combination of double-lined spectroscopic binary with relative astrometry between the two stellar components. Yields orbital parallax and stellar masses, as well as luminosities and radii if resolved with interferometry.

This example is taken from Hummel, C., et al. 2001, AJ, 121, 1623, with data from the Mark III, NPOI, PTI, and spectroscopy with CORAVEL.

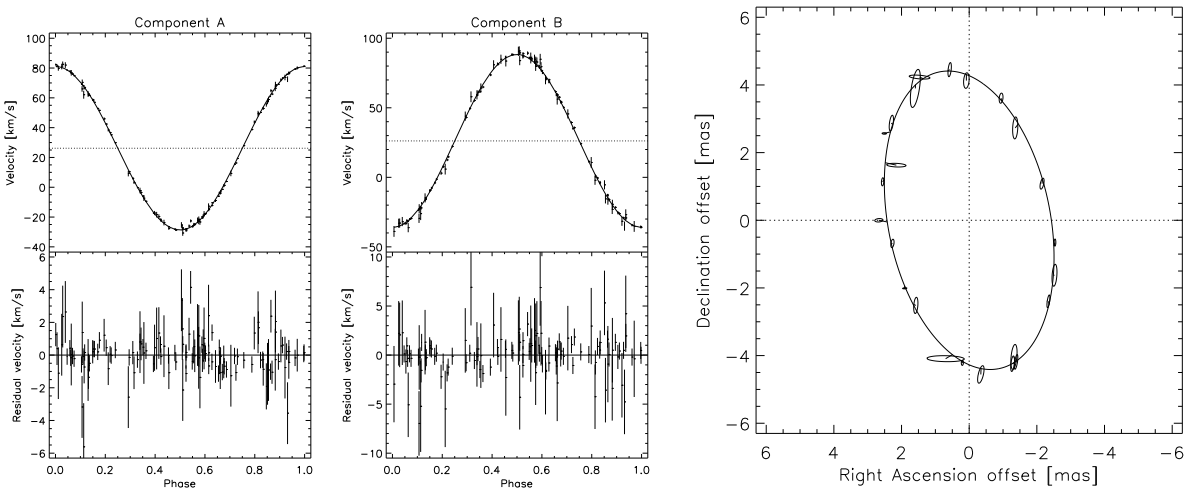

The orbital solution included the masses of the components and was obtained from a combined fit of all available data. This type of fit uses less parameters then a combination of separate fits of the visibilities and radial velocities, and therefore is numerically more stable. Instead of the masses one might include $K_{1,2}$ in the fit, which reduces correlation of parameters but leaves non-linear parameter combination for the determination of the masses.

Parameter	Combined solution
a/mas	4.46 ± 0.01
$i/^\circ$	57.6 ± 0.1
$\Omega/^\circ$ (J2000.0)	191.4 ± 0.1
T (JD−244E4)	10629.831 ± 0.003
e	0
P/days	14.498064 ± 0.000009
$\mathcal{M}_1/\mathcal{M}_\odot$	2.12 ± 0.01
$\mathcal{M}_2/\mathcal{M}_\odot$	1.87 ± 0.01
ϕ_1/mas	1.2
ϕ_2/mas	0.5
$\Delta m_{500\mathrm{nm}}$ [mag]	0.70 ± 0.10
$\Delta m_{550\mathrm{nm}}$ [mag]	0.91 ± 0.05
$\Delta m_{700\mathrm{nm}}$ [mag]	1.05 ± 0.05
$\Delta m_{850\mathrm{nm}}$ [mag]	1.16 ± 0.05
$\Delta m_{2200\mathrm{nm}}$ [mag]	1.49 ± 0.05
γ/(km/s)	26.18 ± 0.05
K_1/(km/s)	54.84
K_2/(km/s)	62.12

Parameter	Primary (F9III)	Secondary (A5m)
D[pc]	41.4 ± 0.1	
$m_V - M_V$	3.09 ± 0.01	
$(B-V)$	0.61 ± 0.06	0.25 ± 0.08
$(R-I)$	0.26 ± 0.05	0.14 ± 0.07
M_V	0.82 ± 0.03	1.73 ± 0.05
M_K	-0.41 ± 0.03	1.08 ± 0.05
T_{eff}/K	6000 ± 200	7600 ± 400
BC	-0.09 ± 0.06	0.02 ± 0.05
M_{bol}	0.73 ± 0.07	1.75 ± 0.07
$L/L_\odot$	39.4 ± 2.4	15.4 ± 1.0
$R/R_\odot$	5.9 ± 0.5	2.2 ± 0.3
D [mas]	1.31 ± 0.23	0.49 ± 0.14
ϕ_{UD} [mas]	1.13 ± 0.06	0.54 ± 0.03

K_1, a'', π: η Pegasi

The more common case of a single-lined spectroscopic binary resolved by interferometry. The knowledge of the parallax enables the sum of the masses be computed in solar units from the relative astrometry, and therefore the individual masses using the one available radial velocity curve. Future astrometric space missions following Hipparcos (FAME, SIM, GAIA) will be able to provide parallaxes of sufficient quality for this to yield astrophysically meaningful stellar parameters.

This example is taken from Hummel, C., et al. 1998, AJ, 116, 2536.

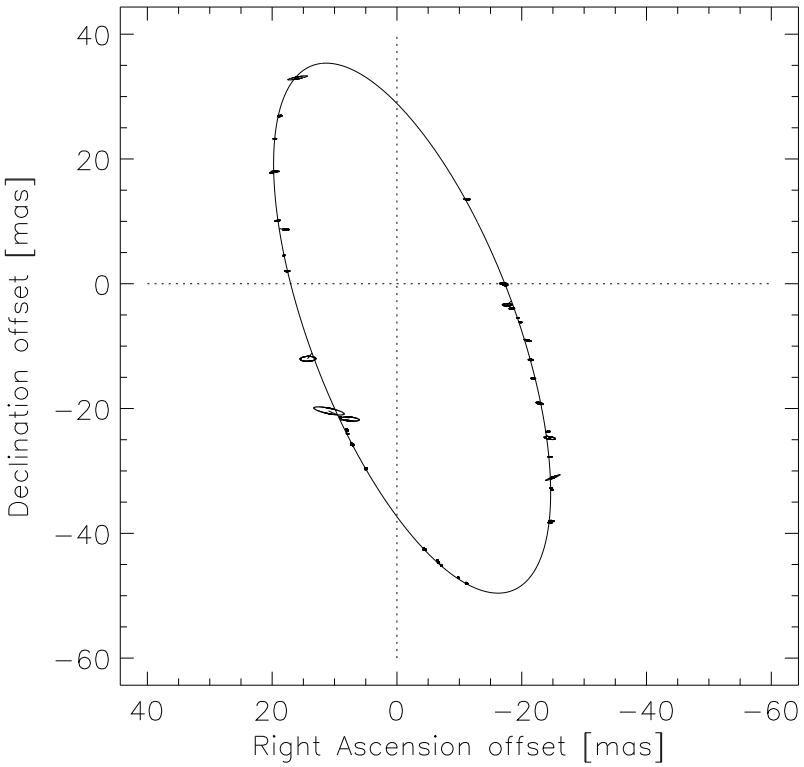

Parameter	Mark III, NPOI, RV	Hipparcos	FAME (estimated)
K_1/(km/s)	14.20 ± 0.19		
a/mas	45.02 ± 0.06		
$a_{\rm PC}$/mas[b]		13.60 ± 0.88	
$i/^\circ$	68.28 ± 0.05	70.6 ± 3.1	
$\Omega/^\circ$ (J2000.0)	20.90 ± 0.04	23.6 ± 3.5[c]	
T (JD−244E4)	7140.3 ± 0.4	7170 ± 9	
e	0.1677 ± 0.0009	0.155 ± 0.016[d]	
$\omega/^\circ$	-5.5 ± 0.1	5.6 ± 5.5[d]	
P/days	817.41 ± 0.04	818 ± 2.2[d]	
π(")		15.18 ± 0.56	15.18 ± 0.05
$\mathcal{M}_1/\mathcal{M}_\odot$		3.2 ± 0.4	3.20 ± 0.04
$\mathcal{M}_2/\mathcal{M}_\odot$		2.0 ± 0.2	1.98 ± 0.03

[a]Systematic error 0.1 mas, [b]Photo center, [c]Orbit of secondary
[d]Adopted from spectroscopy, [e]Adopted from photometry

$a''_{1,2}$, π: σ **Orionis**

Useful for hierarchical multiple systems which provide a reference against which to measure the absolute orbits of the individual stars in the close pair. Adding a parallax measurement will yield masses without any need to measure the radial velocity curves.

The visibility and closure phase data shown below are from two scans taken with NPOI using three baselines on 2000, October 18. The data are plotted versus channel number with solid lines indicating a preliminary model for the triple system. Initial estimates for separation and position angle of the wide pair were taken from the WDS and Hipparcos, and subsequently adjusted. The close pair is in a very eccentric orbit with a period of some 10 days.

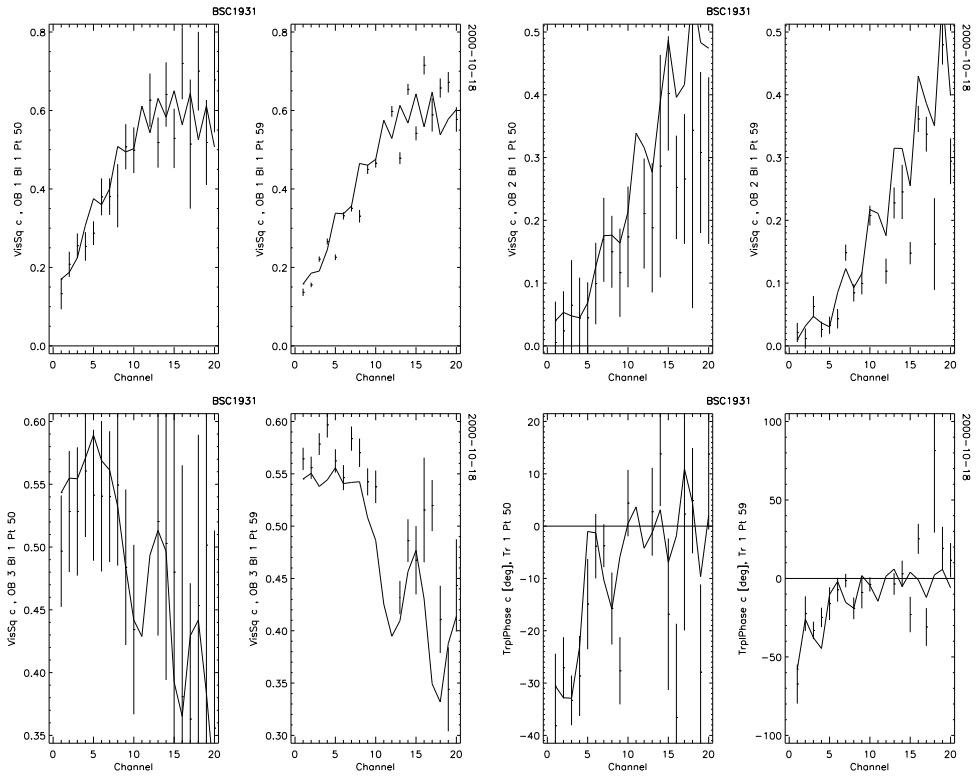

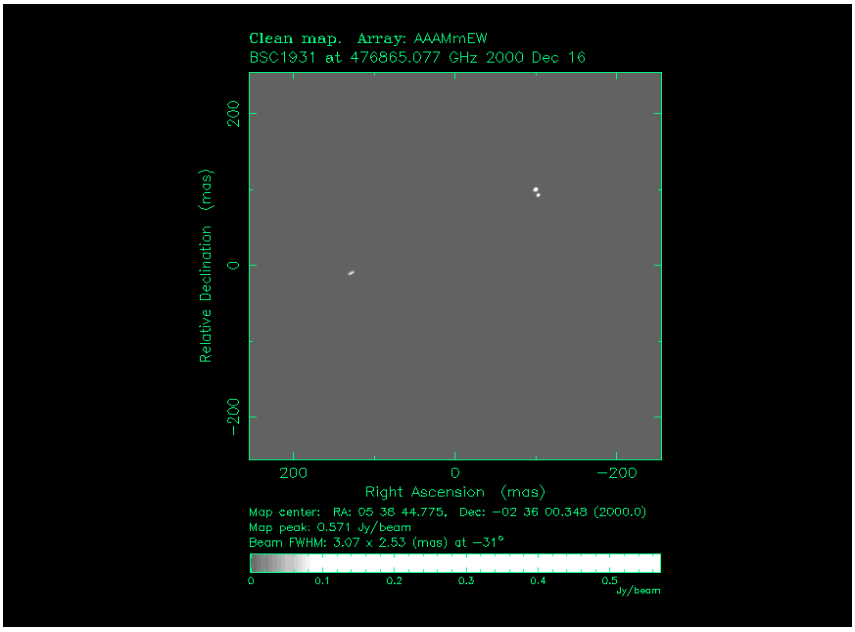

The image on the right is from a simulation of a six-station observation with NPOI using 20 channels. (Courtesy of Difmap [M. Shepherd]). The slight elongation of the distant component is due to bandwidth smearing.

$K_{1,2}$, $m(t)$, a'': ζ Aurigae

Double-lined eclipsing binaries have been the reliable source of high-accuracy stellar masses and radii. If an interferometric orbit is available, the distance estimate can be improved.

The example is taken from Bennett, P., et al. 1996, ApJ, 471, 454, with data from the GHRS on HST, photometry, and the Mark III.

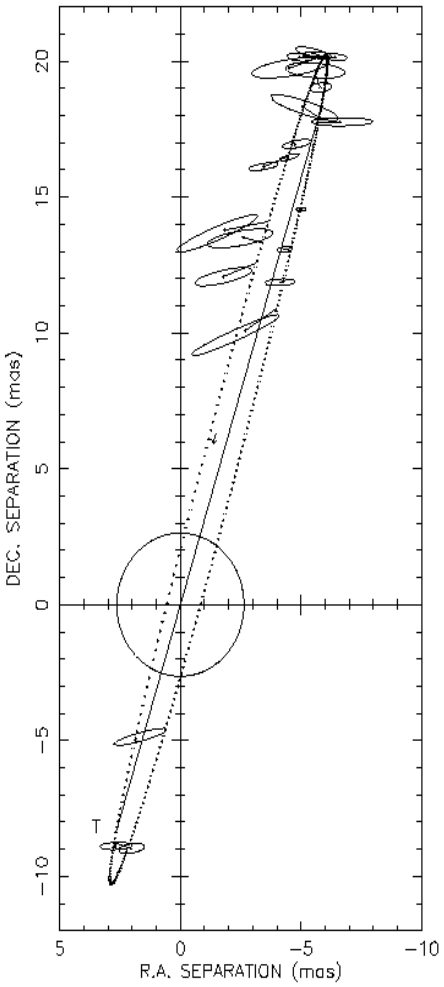

The orbit of ζ Aurigae is shown on the right. The large circle outlines the size of the K supergiant primary as measured by interferometry. The secondary is an unresolved main-sequence B star.

Below left, we show the visibility amplitudes plotted versus the projected baseline length, with the upper envelope set by the apparent size of the primary.

Below right we show the U light curve of the eclipse. From the photometry one can derive the inclination angle (an independent estimate from interferometry) and the radii of the individual stars in units of the semi-major axis of the orbit.

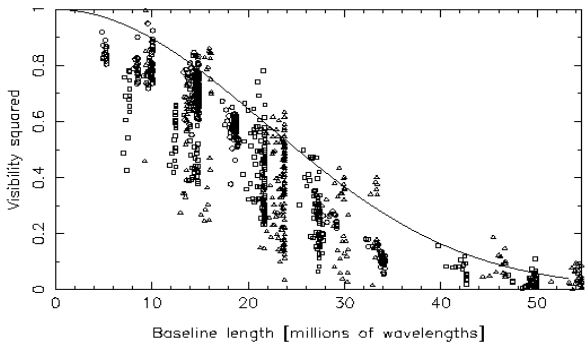

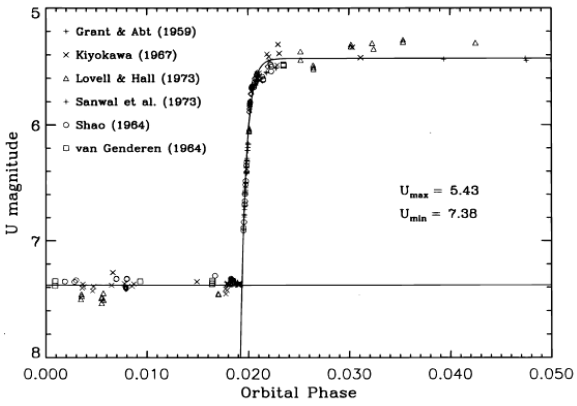

Orbital elements of a double star

The (relative) orbital motions of two components in a binary are fully described using seven orbital elements (if apsidal motion is negligible). These are (from W. Heintz, 1978, Double Stars [Dordrecht: Reidel]):

- a: semi-major axis of the true orbit
- e: (numerical) eccentricity
- i: inclination, direct (towards increasing position angle) motion for $i < 90°$, retrograde otherwise
- ω: periastron angle, reckoned in the direction of motion
- Ω: node, ascending if radial velocity of the component is positive
- P: period
- T: epoch of periastron passage

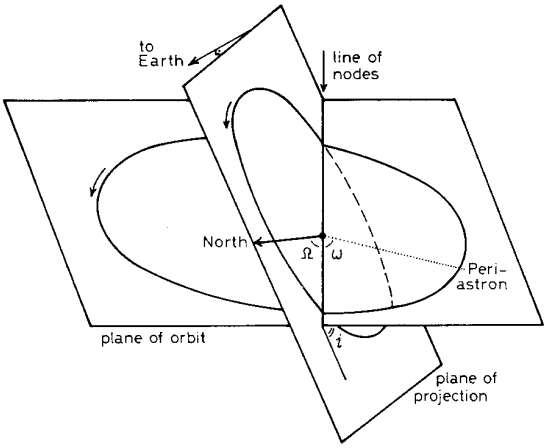

Fig. 7. The true and the projected orbits of a visual binary, and its geometrical elements.

In the apparent ellipse of the orbit, the zero point O is in the primary star, M is the center of the ellipse, π the periastron, and $M\pi$ is the projection of the semi-major axis, so that the eccentricity $e = MO/M\pi$.

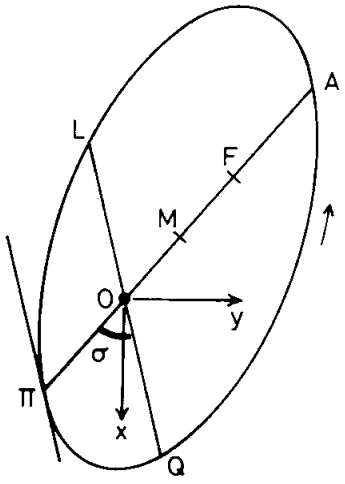

Fig. 11. The geometry of the apparent orbital ellipse.

Kepler's equation

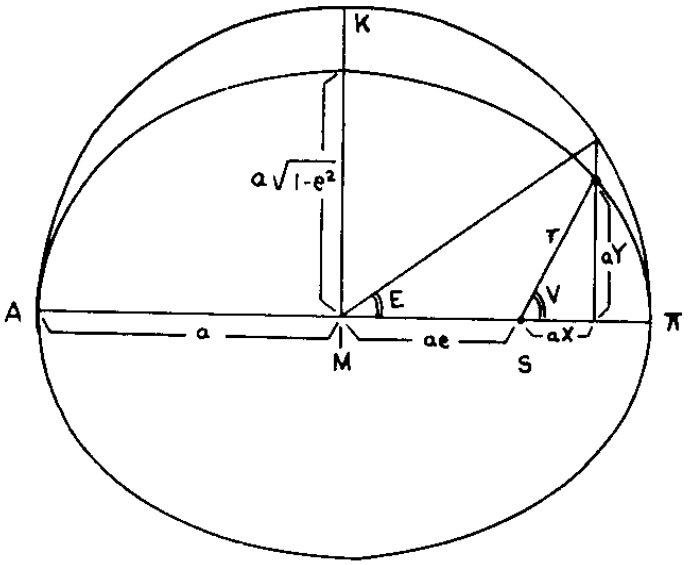

Fig. 8. The definition of quantities in the elliptical orbit and in Kepler's equation.

Computation of (ρ, θ) at epoch JD:

- M: mean anomaly, `M=2*!pi*((JD-t) mod p)/p`
- E: eccentric anomaly, $M = E - e \sin E$ (Kepler's equation),
  `E=M+e*sin(M)+e^2/2*sin(2*M)`
  `for k=0,4 do E=E+(M-E+e*sin(E))/(1-e*cos(E))`
- ν: true anomaly,
  `nu=2*atan(sqrt((1+e)/(1-e))*sin(E/2),cos(E/2))`
- (ρ, θ):
  - `alpha=nu+w`
  - `theta=atan(sin(alpha)*cos(i),cos(alpha))+n`
  - `rho=a*(1-e^2)/(1+e*cos(T))*sqrt(cos(alpha)^2+sin(alpha)^2*cos(i)^2)`

with `n`$= \Omega$ and `w`$= \omega$. Text in `this font` is IDL code, but use different symbols for `e` and `E` (IDL is not case sensitive).

Orbital motion

Long baseline interferometers provide the resolution to resolve many of the spectroscopic binaries. It is a simple selection effect that these binaries tend to have short orbital periods which means that orbital motion during the interferometric aperture synthesis can be significant.

Below is the example of β Aurigae (taken from Hummel, C., et al. 1995, AJ, 110, 376) which has an orbital period of about 4 days. Data were taken with the Mark III in three filters, and visibilities from one of the night's data are shown. The model values are from a direct fit of the orbital elements to the visibility data.

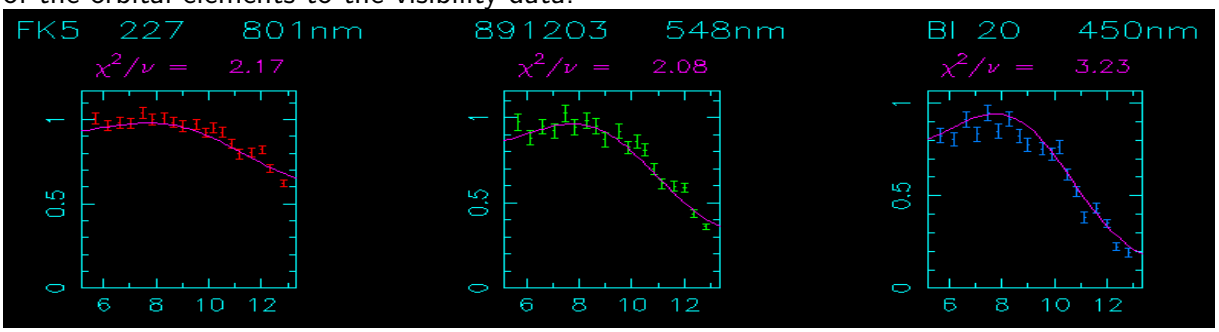

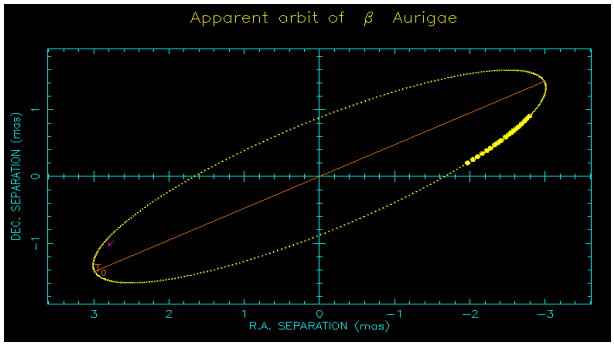

The orbital phase covered by the visiblity measurements in this particular night is shown to the right and exhibits a significant spread.

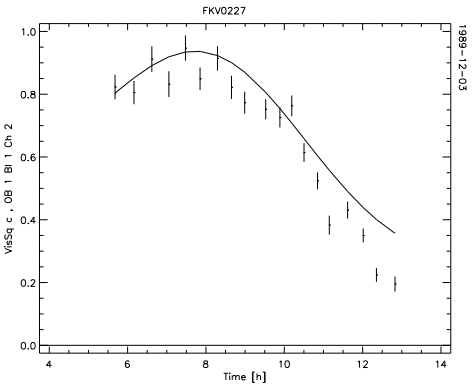

The fit to the blue visibilities shown to the right is for a constant $(\rho, \theta) = (2.8, 281^\circ)$ and clearly inferior to the fit including orbital motion (shown above). However, a better fit can be achieved by adjusting the relative position to $(\rho, \theta) = (3.3, 280^\circ)$, but now inconsistent with the orbit! Only a direct fit to the visibilities with good phase coverage will yield unbiased orbital elements.

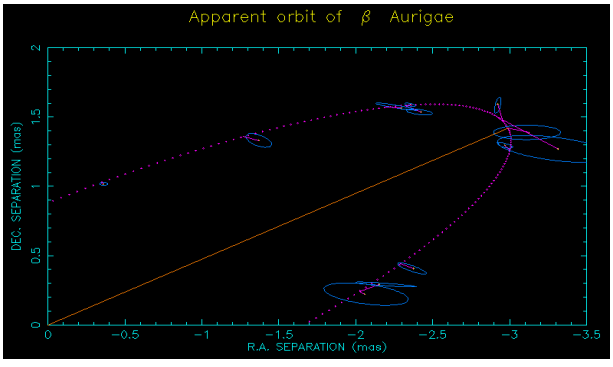

In order to provide a visual representation of quantity and quality of the data, one possible way is to plot separations and position angles with the orbital solution. These intermediate astrometric results have been derived accounting for motion by using the orbital solution.

Determinacy of the orbit

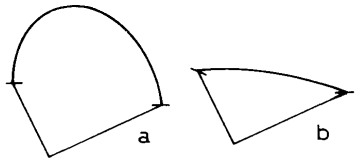

Fig. 9. Determinacy of an ellipse from a short observed arc: fair in case *a*, undefined in *b*.

The (squared) visibility on a single baseline measures position angles subject to a 180° ambiguity (quadrant error), which can lead to highly eccentric orbit solutions in local minima of the goodness-of-fit surface.

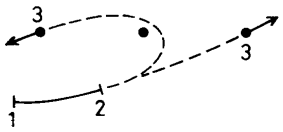

Fig. 10. The ambiguity of quadrant.

In order to ascertain that the data uniquely constrain the parameters of the visual orbit one can map out the χ^2 hyper-surface in an adequately large neighborhood of the putative global minimum. The example below is taken from Boden, A., et al. 1999, ApJ, 515, 356, who describe work done with the PTI on ι Pegasi, an almost edge-on orbit.

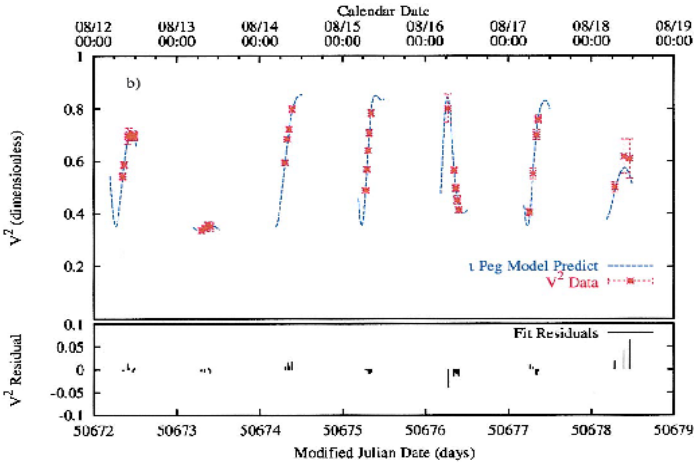

The visibility data of seven (out of 11) nights plotted versus date and time, with the model prediction.

Shown below are the χ^2/DOF fit surfaces for ι Peg data. Two surfaces are shown, on in the subspace of orbit semimajor axis and relative component brightness, the other in the subspace of orbital inclination and longitude of the ascending node. The insets are color contour maps providing closeups of the minima regions.

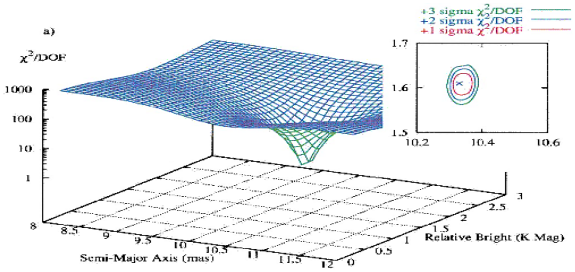

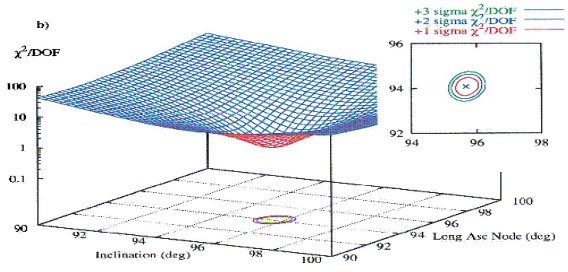

Hybrid mapping

Here are flow diagrams of the two major imaging strategies developed for Earth-rotation aperture synthesis in radio astronomy. These techniques are known as hybrid mapping since the use of closure phases requires the self-calibration of the baselines phases with a model, which in turn depends on the data! This model is iteratively improved through the application of the CLEAN algorithm. Hybrid mapping converges if the source structure is sufficiently simple.

The "classic" scheme derives the new model in its entirety every major cycle through CLEAN.

(Conventional) Hybrid mapping

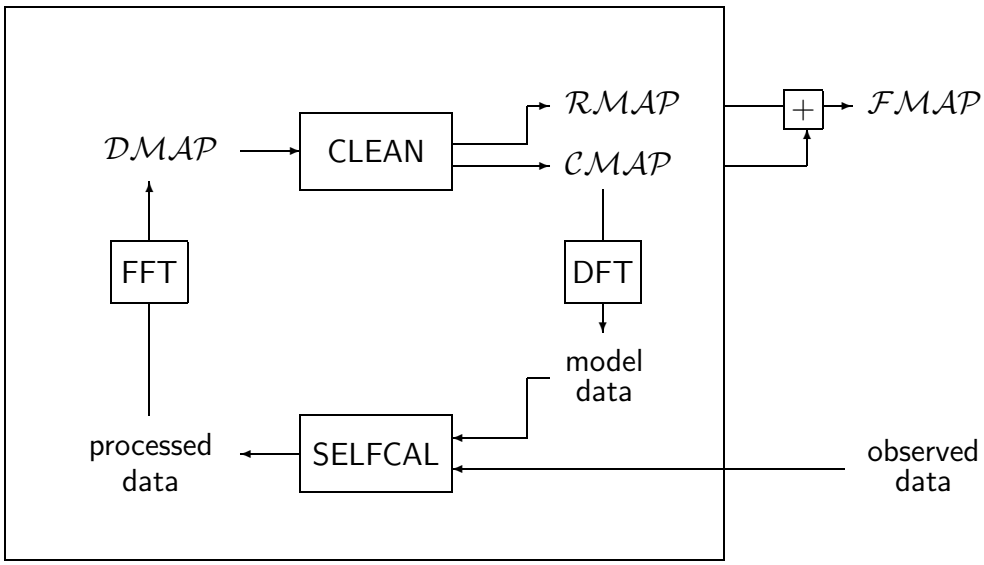

The difference mapping algorithm assembles a model successively by self-calibrating the data every time a few CLEAN iterations have been performed on the residual map of the previous cycle. The residual map is the Fourier transform of the self-calibrated data *minus* the current model. This algorithm can therefore be started off with a source model (e.g. a limb darkened disk) to self-calibrate the phases, leaving the imaging of the surface feature to hybrid mapping.

Difference mapping

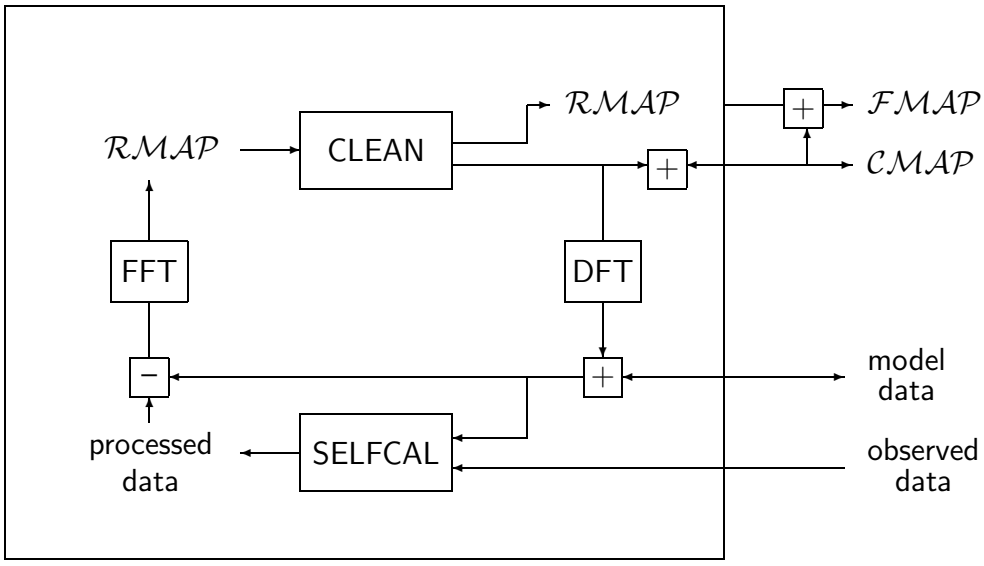

Imaging composite spectrum binaries – 1

Considering the more important aspect of composite spectrum binaries, that is the difference in spectral type the two components may have, we are challenged to image a structure which depends on wavelength. Rather than imaging every channel of a multi-channel interferometer separately, we combine the data in order to improve the synthesized beam. The algorithm outlined below is capable of reconstructing an image by introducing the effective temperature of a CLEAN component as an additional parameter to account for the wavelength dependence of the stellar structure.

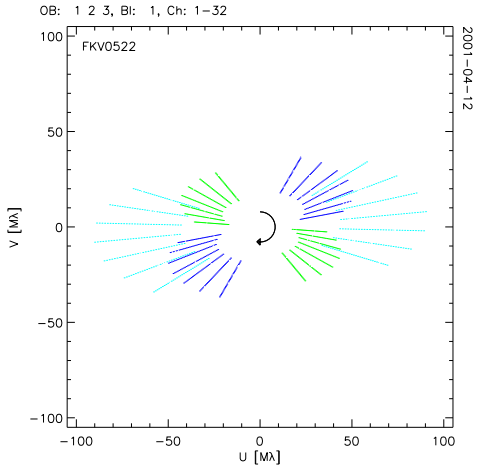

Here is the aperture coverage of a simulated three baseline observation of NPOI with 32 channels. Each radial line is composed of the 32 visibilities measured on a single baseline at one time with the spectrometer.

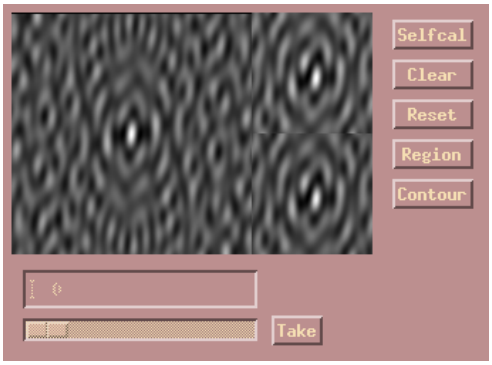

The large square map to the right shows the PSF of just two adjacent channels. Note the rather high level of the sidelobes. Also note that the secondary (in the small maps) is barely visible before CLEAN.

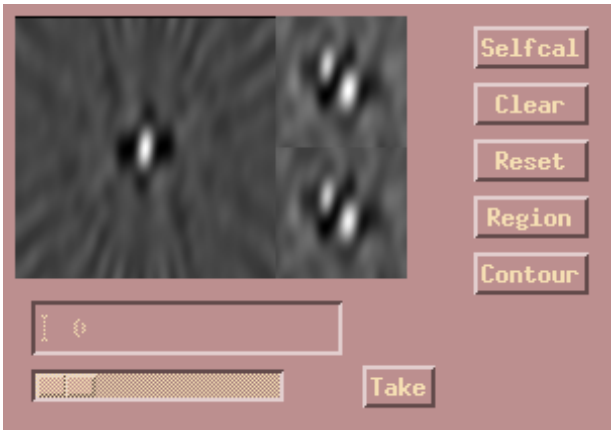

On the right we see the dirty (synthesized) beam, DB (also called PSF in the optical, or antenna diagram in the radio) based on data of all channels combined. However, we keep each DB_λ separate for the following computations. The small images to the right of the DB are the dirty map (DM, bottom) and final map (FM, top). They have half the size of the DB by design. The DM changes into the residual map (RM) after the subtraction of CLEAN components and the application of self-cal.

Imaging composite spectrum binaries – 2

These are the results from an imaging process which doesn't account for the different colors of the stars we chose in this example. Note the rather high level of remaining sidelobe structure.

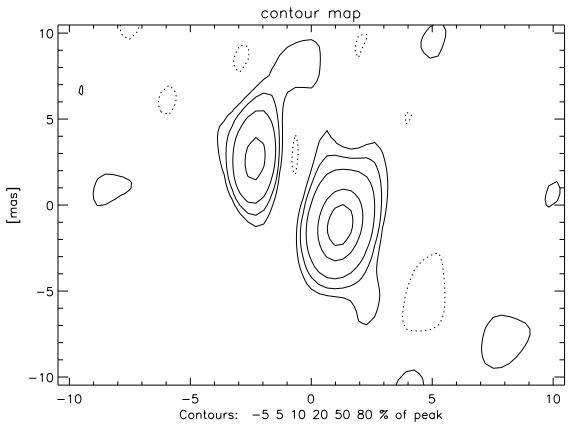

By introducing the effective temperature as an additional parameter, but allowing only two different values depending on the region in the map, we can arrive at a proper solution of the imaging problem. The CLEAN algorithm is modified such that in each iteration, instead of subtracting the combined DB we subtract each DB_λ weighted with the stellar flux in that channel of a CLEAN component given its specific temperature, normalized by the total flux over all areas.